Structural and Dynamics Aspects of ASC Speck Assembly

Ali Can Sahillioglu,[2,4] Fidan Sumbul,[1,4] Nesrin Ozoren,[2,3,5,*] and Turkan Haliloglu[1,3,5,*]

[1]Department of Chemical Engineering and Polymer Research Center, Bogazici University, 34470 Istanbul, Turkey
[2]Department of Molecular Biology and Genetics, Apoptosis and Cancer Immunology Laboratory (AKIL), Bogazici University, 34470 Istanbul, Turkey
[3]Center for Life Sciences and Technologies, Bogazici University, 34470 Istanbul, Turkey
[4]Co-first author
[5]Co-senior author
*Correspondence: nesrin.ozoren@boun.edu.tr (N.O.), haliloglut@boun.edu.tr (T.H.)
http://dx.doi.org/10.1016/j.str.2014.09.011

SUMMARY

Activation of the inflammasome is accompanied by rapid formation of a micrometer-sized perinuclear structure called the ASC speck, a platform for caspase-1 activity. The ASC speck is often referred to as an aggregate and shares certain features with aggresomes. It is thus an open question whether the ASC speck formation takes place via nonspecific aggregation of hydrophobic patches or specific interactions of its domains; PYD and CARD, which belong to the death fold superfamily. Bringing together structure and dynamics studies using the Gaussian network model of PYD and CARD, and molecular dynamics simulations of the wild-type and in silico mutated PYD, with the mutational analysis on the ASC structure and its separate domains in human cells, we show that the ASC speck is an organized structure with at least two levels of distinct compaction mechanisms based on the specific interactions of PYD and CARD.

INTRODUCTION

The inflammasome complexes form upon detection of intracellular pathogen-associated molecular patterns, as well as damage-associated molecular patterns (Gross et al., 2011; Leemans et al., 2011). Pathogen-associated molecular patterns are detected by cytoplasmic pattern recognition receptors such as NLRP3, NLRC4, and AIM2, which become components of inflammasomes (Latz et al., 2013). NLRP3 inflammasome is activated by wide range of stimuli such as pore-forming toxins, particulate materials, and extracellular ATP (Gross et al., 2011). Potassium efflux, lysosomal damage, and reactive oxygen species derived from mitochondria have been proposed for downstream signaling of the NRLP3 inflammasome (Hornung and Latz, 2010; Muñoz-Planillo et al., 2013; Zhou et al., 2011). For NLRP3 and AIM2 inflammasomes, the ASC protein functions as an adaptor that bridges procaspase-1 to the receptors, whereas NLRC4 can directly interact with procaspase-1 (Schroder and Tschopp,

2010). According to an accepted theoretical model (Schroder and Tschopp, 2010), oligomerization of inflammasome receptors is followed by the recruitment of ASC that associates with procaspase-1. Procaspase-1 proteins that are in proximity undergo autocleavage and become active. The mature caspase-1 is then capable of processing proIL-1beta and proIL-18 that are subsequently secreted from the cell (Latz et al., 2013). Activation of NLRP3, NLRC4, and AIM2 inflammasomes is known to be accompanied by rapid formation of a micrometer-sized compact perinuclear structure called the ASC speck/ASC foci/pyroptosome (Broz et al., 2010a, 2010b; Fernandes-Alnemri et al., 2007; Jones et al., 2010). The ASC speck was proposed to be the platform for caspase-1 activity (Fernandes-Alnemri et al., 2007).

The ASC protein contains two domains: N-terminal PYD (amino acids M1-T89) and C-terminal CARD (residues H113-S195), connected by a flexible 23-residue linker (amino acids H90-L112). PYD and CARD are members of death-fold superfamily domains (de Alba, 2009). Both domains are composed of structurally independent six-helix bundle motifs (Figure 1). The linker allows a back-to-back orientation of the two domains and may facilitate interactions with multiple partners. Any nuclear magnetic resonance (NMR)-derived contacts are not observed between either of these two death domains or any domain and the linker, which indicate that PYD and CARD do not directly interact with each other (de Alba, 2009). There are some structural differences between the PYDs of different proteins; however, the ASC2 protein (Protein Data Bank [PDB] ID 2HM2), which consists of only a pyrin domain, has a very high structural similarity with the PYD of full-length ASC (Natarajan et al., 2006). This may indicate that the presence of CARD does not affect the structure of PYD. However, the 3D structure of the CARD-CARD complex (Qin et al., 1999) (CARD of human APAF1 and human Caspase-9; PDB ID 3YGS) shows that there are some structural differences between the CARD of those proteins and the CARD of ASC, particularly at the CARD-CARD interface.

Death-fold superfamily domains are characteristically present in proteins involved in inflammatory and apoptotic pathways. Proteins containing these domains interact with each other via homotypic interactions. ASC interacts with procaspase-1 and NLRC4 by establishing homotypic interactions using the CARD present in these proteins. Similarly, ASC interacts with NLRP3
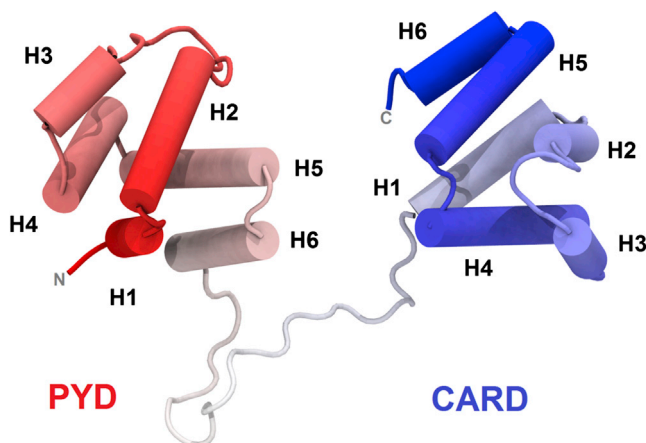
Figure 1. The Structure of ASC
NMR structure of full-length human ASC protein (de Alba, 2009) (PDB ID: 2KN6) with domains and secondary structural elements labeled.

and AIM2 via homotypic interactions using PYD (Schroder and Tschopp, 2010). The PYD and CARD of ASC form filament structures when overexpressed as separate domains (Masumoto et al., 2001). The PYD-filament formation was suggested as a result of back-to-back assembly of two oppositely charged surfaces on PYD. This interaction is called type I interaction mode, which uses helices H1 and H4 at one surface and helices H2 and H3 on the other surface (Liepinsh et al., 2003; Vajjhala et al., 2012). The second proposed mode, type II interaction mode, in this superfamily is observed between helix H4 and the H4 and H5 loop at one surface and the H5 and H6 loop of the opposing surface. Another mode of interaction, type III interaction mode, is observed between helix H3 at one surface and the loops of H1 and H2 and H3 and H4 on the other surface. Alternative interaction modes (type II and type III) were experimentally shown for other members of the death-fold superfamily domains containing proteins (Kersse et al., 2011; Lin et al., 2010; Park et al., 2007; Wang et al., 2010). A mutational screen on the CARD of ASC has identified multiple surfaces important in the ASC speck formation (Proell et al., 2013). Finally, the cryoelectron microscopy (cryo-EM) structure of PYD filaments was published while the present manuscript was in preparation (Lu et al., 2014). Type III interaction mode surfaces appear slightly different in this structure; the loops H1 and H2 and H2 and H3 form the opposite surfaces.

The ASC speck structurally resembles aggresomes by its cellular localization, size, compact shape, ubiquitination, sensitivity to microtubule depolymerizing drugs, association with proteasomes, and colocalization with vimentin and microtubule organizing center (Balci-Peynircioglu et al., 2008; Cheng et al., 2010; Johnston et al., 1998; Shi et al., 2012). Few differences between the ASC speck and aggresome include formation kinetics because the ASC speck formation is rapid (takes place in few minutes) compared to hours-long aggresome formation (Fernandes-Alnemri et al., 2007; Richards et al., 2001). The events that trigger formation of these structures are also different, because aggresome forms as a result of cellular stress or protein misfolding, whereas the ASC speck formation requires inflammasome activation (Johnston et al., 1998; Miao et al., 2011).

The resemblance between the ASC speck and aggresome raises the question as to whether the ASC speck formation is a result of specific interactions between PYD and CARD or simply aggregation of hydrophobic patches of ASC proteins. To address this question, we performed structure- and dynamics-based analyses on the ASC protein to predict dynamically important amino acids that could be plausible for the binding interactions of PYD and CARD, which were then subjected to a mutational analysis. Our results indicate that the ASC speck formation is based on specific homophilic but not heterophilic interactions by PYD and CARD separately. We propose a model in which filament formation is the first level of organization in the ASC speck. Filaments further compact in a higher organization level, which can be inhibited by the L25A mutation. Finally, PYD uses alternative interaction modes other than type I that might be important in compaction of the ASC speck, which is presented with a mechanistic view based on the dynamic characteristics of PYD.
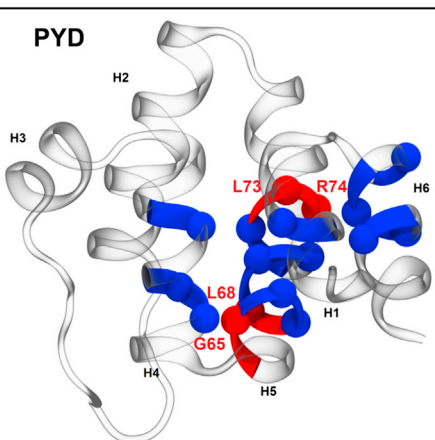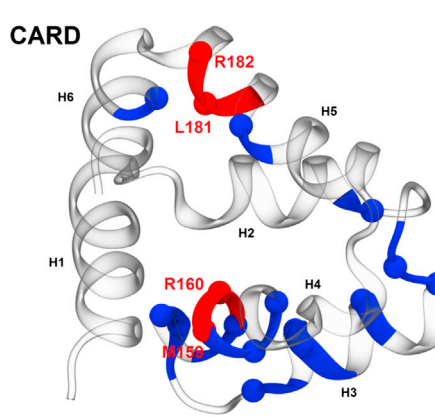
RESULTS

Prediction of Binding Core Amino Acids on ASC by Fast Modes of Motion

Amino acids that fluctuate in high frequency/fast modes by Gaussian network model (GNM) are kinetically hot spots shown to have structural and functional importance (Bahar et al., 1998; Ertekin et al., 2006; Haliloglu et al., 1997, 2008; Haliloglu and Erman, 2009; Ozbek et al., 2010, 2013). Binding sites are associated with high as well as low stability regions (Luque and Freire, 2000; Swapna et al., 2012). The folding and binding core amino acids associate with the high frequency fluctuations, which respectively may infer stability of tertiary fold or/and local regions. Twenty-two amino acids from PYD and 20 amino acids from CARD were identified by the fast modes of motion (Figures S2A and S2B available online), which are expected to be highly conserved, relatively buried, and clustered in space. With the conservation score ≥ 4 (Landau et al., 2005), 16 and 17 amino acids, respectively, remained as candidates for the binding core amino acids of the ASC protein (Figure 2). We initially proposed G65, L68, L73, and R74 from PYD; M159, R160, L181, and R182 from the CARD; and a double mutation L68-R160 from both domains of the ASC protein.

Single Amino Acid Mutations Change the Assembly of the ASC Speck

A series of point mutations in the ASC protein based on the fast modes of dynamics (Figure 2) were created to explore whether these amino acids that are plausible for the intrinsic binding behavior of the PYD and CARD are indeed crucial for the ASC speck formation. In addition, single point mutations into alanine were also generated based on the correlation of previously studied amino acids of PYD (Vajjhala et al., 2012) with the key sites of the dynamics; E13, E19, K21, L25, K26, R41A, D48, D51, E62, and E67 were related to the hinges of the global dynamics (Figure 3) and D51A and E67A also were associated with the high-frequency fluctuations (Figure 2). L25 and K26 are not hinges but only closely positioned with the hinge R41 in the structure. Additionally, double mutation K26A-R160A was also considered. In total, 18 amino acids were mutated into alanine and two double mutations were generated.

High frequency fluctuating residues with conservation scores≥4		
	I8(8)	H1
	T53(7), L56(7), V57(6)	H4
Panel A (PYD)	**G65**(7), _E67(5)_, **_L68_**(9)**, T69(8), A70(4), V72(8), **_L73_**(9)**, **R74**(4)	H5
	79(4), E80(4), A82(9), L85(9)	H6
	L141(9), T142(5)	Loop H2&H3
	Y146(9), V149(8), R150(8)	H3
	E152(5)	Loop H3&H4
Panel B (CARD)	N155(6), P156(7), K158(6), **M159**(9)*, **R160**(9)*, K161(7), L162(9)	H4
	L178(6), **_L181_**(9), **_R182_**(4)	H5
	188(9)	H6

Bold: suggested for mutation,
Underlined: mutated _in vivo_ in full length ASC,
Italic: mutated _in vivo_ in truncated domain,

(X): Conservation scores (9:highly conserved, 1:highly variable)

*: _in vivo_ mutation changed speck structure into filament in full length ASC,
**: _in vivo_ mutation in truncated PYD domain inhibited filament formation as well as inhibition of speck formation in full length ASC.

Figure 2. High-Frequency Fluctuating Amino Acids

High-frequency fluctuating amino acids in average three fastest GNM modes on separate PYD and CARD filtered with evolutionary conservation scores: 16 of 22 and 17 of 20 high frequency fluctuating amino acids in total, respectively, appear with the conservation scores ≥4; with the continuous conservation values partitioned into a discrete scale of nine bins, a grade of 1 indicates a highly variable amino acid position and grade 9 is highly conserved (Landau et al., 2005). See also Figure S2.

We hypothesized that filament formation by the mutated ASC constructs is a result of the remaining intact domain because the separate PYD and CARD, each can form similar filaments when expressed as separate domains (Masumoto et al., 2001). To prove this theory, we generated two combinations of double mutations targeting both domains of ASC (K26A-R160A and L68A-R160A). Double mutant EGFP-ASC constructs showed a diffused expression pattern throughout the cell and failed to form either filaments or ASC specks (Table 1 and Figure 4G).

Strikingly, the L25A mutant displayed a different phenotype, which appears as an intermediate between the ASC speck and filaments formed by some mutant ASC constructs. The structure formed by the L25A mutant ASC is referred to as "Medusa's head" phenotype in this study. It is a perinuclear structure with a size comparable to the ASC speck and has apparent filament extensions pointing outward from its core (Figure 4H). ASC is a relatively conserved protein with 71.8% sequence identity between the human and mouse versions. However, L25 is not conserved and there is a methionine amino acid at this position in mouse ASC. Because compact-shaped ASC specks have been reported in mouse studies, we hypothesized that a methionine can substitute the leucine amino acid at this position in human ASC. Indeed, L25M-mutated EGFP-ASC recovered the compact, globular shape of the ASC speck (Figure 4I).

If we consider the set of 11 mutations that disrupt the speck formation, the fast and slow modes dynamics predict and/or provide a mechanistic and dynamic aspect in ten of these mutations. Amino acids L68 and L73 from PYD and M159 and R160 from CARD are among the high-frequency fluctuating amino acids as were the amino acids L68 and R160 in double mutations L68A-R160A and K26A-R160A. D51 is a neighbor to T53, which is also a high-frequency fluctuating amino acid. Amino acids E13, E19, K21, R41, and D48 are at the hinge sites of the global
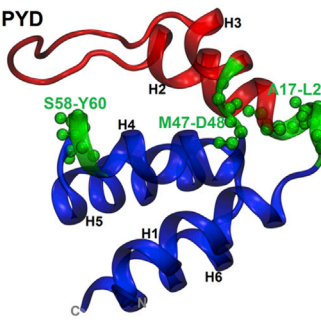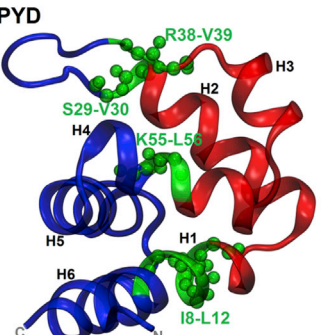
Plasmids encoding for each of the mutated ASC as a fusion protein with EGFP were transfected into HEK293T cells, and confocal microscopy was used to observe and evaluate the ASC speck formation. EGFP-ASC overexpression in HEK293T cells gives rise to spontaneous ASC speck formation, similar to the ASC specks formed in human macrophage cells after NLRP3 inflammasome activation (Figures S1A–S1C). Seven of the 18 single amino acid mutations did not have an effect on the ASC speck formation. However, 11 single amino acid mutations (E13A, E19A, K21A, K26A, R41A, D48A, D51A, L68A, L73A, M159A, and R160A) disrupted the ASC speck (Table 1 and Figures 4B–4E). These mutated ASC constructs formed filaments extending throughout the cell very similar to the filaments formed by the expression of either PYD or CARD domains alone, or the short isoform (Matsushita et al., 2009) of ASC (Figure 4F).

Residue IDs			
(r_cut=7Å)	(r_cut=10Å)		
*E13(8)***, N14(5)	A17(5), E18(4), *E19(5)***, L20(4)	Loop H1&H2	
_D48(8)_**¹, A49(4)	M47(7), _D48(8)_**¹	Loop H3&H4	**Panel A (Slow 1)**
	S58(7), F59(4), Y60(8)	Loop H4&H5	
	I8(8), L9(5), A11(6), L12(9)	H1	
L28(5), S29(7)	S29(7), V30(4)	Loop H2&H3	
V39(9), P40(7)	R38(5), V39(9)	Loop H2&H3	**Panel B (Slow 2)**
	K55(7), L56(7)	H4	
_E62(7)_, T63(1), Y64(3), **G65**(7), A66(3)		H5	

Bold: suggested for mutation,
Underlined: mutated *in vivo* in full length ASC,
Italic: mutated *in vivo* in truncated domain,

*: *in vivo* mutation changed speck structure into filament in full length ASC,
**: *in vivo* mutation in truncated PYD domain inhibited filament formation as well as inhibition of speck formation in full length ASC.
¹ : mutated truncated domain co-localize with wild type truncated domain

(X): Conservation scores (9:highly conserved, 1:highly variable)

Figure 3. Hinge Residues of GNM Modes
Hinge residues of the slowest (A) and second slowest (B) modes of GNM by both 7 Å and 10 Å r_cut, are shown on PYD (green backbone spheres). Dynamic domains identified by the hinge axes/plane at 10 Å are red and blue. See also Figure S2.

disrupt the PYD folding (Srimathi et al., 2008; Vajjhala et al., 2012). For K26A, L68A, L73A, M159A, and R160A mutations, we expressed mutated ASC proteins without EGFP fusion to check their stability in cells (Figure S1E). L68A- and L73A-mutated full-length ASC proteins were expressed only poorly, suggesting that these two mutations might affect mainly folding stability. On the other hand, D75 is a binding site of type I interaction mode based on the recent cryo-EM structure (Lu et al., 2014) and further R75A on pyrin PYD (R74A in ASC PYD) affected the pyrin PYD-ASC PYD association, implying a close association of the folding and binding residues here.

Furthermore, the amino acids that show high-frequency fluctuations (Figure 2) but not tested in the present work (T53, L56, V57, A70, and Q79) were associated with ASC-PYD self-association or its binding to other PYDs (Vajjhala et al., 2012, 2014; Lu et al., 2014). Together with L68A and L73A, which lead to significant stability decrease (Figure S1E), H5 is possibly an important site of structural stability and some binding interactions.

Parallel Effects of Mutations on Full-Length ASC and Its Separate Domains

PYD and CARD form filaments via homotypic interaction when expressed as separate domains (Masumoto et al., 2001). We labeled PYD and CARD with green and red fluorescent proteins, respectively. We demonstrate that PYD and CARD form mutually exclusive filaments when expressed in the same cell, which indicates that the PYD-PYD and CARD-CARD interactions are highly specific (Figure 5A).

Parallel sets of mutations (Table S1) were carried out on separate PYD and CARD constructs, and the effects of the mutants were analyzed according to presence or loss-of-filament formation. We observe that ASC speck disrupting mutations in the full-length protein construct also inhibit filament formation of separate PYD and CARD domain constructs and vice versa (Figures 5B–5D). Mutated PYD constructs show a gradual inhibition in the filament formation. Whereas E13A, K21A, K26A, D51A, and L73A mutations on the PYD inhibited filament formation frequency by varying degrees, E19A, R41A, D48A, and L68A

motion of PYD (Figure 3), which will be discussed. On the other hand, mutations G65A, R74A, L181A, and R182A did not affect the speck formation. G65 and K181 are among highly conserved amino acids (Landau et al., 2005). L181A and R182A may relate another functional site. Alanine is yet observed at positions G65 and R74 within the ASC homologs' structures and thus another substitution might show an effect. On the other hand, the R74 corresponding position on pyrin PYD (R75A) was shown to disrupt the pyrin PYD-ASC PYD association (Vajjhala et al., 2014). E62A and E67A, which were dynamically plausible for a functional role but did not show any effect, were false-positive results with respect to structural/functional attributes focused here.

For the mutations that were carried out in the present work and affected the ASC speck formation, there is evidence in the literature that E13A, L25A, K21A, R41A, and D48A mutations do not

Table 1. Summary of ASC Variants' Phenotypes

ASC Variant	Phenotype	Location
WT long isoform	speck	–
E13A	filament	PYD
E19A	filament	PYD
K21A	filament	PYD
L25A	Medusa's head	PYD
L25M	speck	PYD
K26A	filament	PYD
R41A	filament	PYD
D48A	filament	PYD
D51A	filament	PYD
E62A	speck	PYD
G65A	speck	PYD
E67A	speck	PYD
L68A	filament	PYD
L73A	filament	PYD
R74A	speck	PYD
M159A	filament	CARD
R160A	filament	CARD
L181A	speck	CARD
R182A	speck	CARD
K26A-R160	soluble	PYD + CARD
L68A-R160	soluble	PYD + CARD
Short isoform	filament	no linker

Phenotypes of two isoforms, 19 single site-directed mutations and two double mutations are summarized. Indicated ASC variants were labeled with EGFP, transfected into HEK293T cells, and observed with confocal microscopy as in Figure 4.

mutations on PYD and M159, R160A mutations on CARD completely abolished filament formation (Figure 5D). The L25A mutation on the separate PYD did not alter the filament formation frequency, which indicates that this mutation does not affect PYD-PYD interactions. Note that the atypical L25A mutation on the full-length ASC protein formed a Medusa's head phenotype. Mutant EGFP-PYD- and mCherry-CARD-expressing cells were analyzed by western blotting, and the mutant constructs were found to result in expression of same-size protein products at comparable levels to wild-type (WT) constructs except for L68A and L73A (Figures 5E and 5F).

Type I Is Not the Only Effective Interaction Mode in PYD-PYD Interactions

The putative type I mode interaction surfaces with helices H1 and H4 at one surface and H2 and H3 at the other surface of PYD have positive and negative electrostatic surface potentials, respectively, and the PYD filament formation was proposed to be based on the electrostatic interactions between these surfaces (Liepinsh et al., 2003). Recently, a mutagenesis analysis provided the evidence for the presence of type I mode for the PYD of ASC (Vajjhala et al., 2012). Other members of the death-fold superfamily were shown to possess alternative interaction modes (Kersse et al., 2011). We designed experiments to find out whether type I is the only possible interaction mode between PYDs.

Type I interaction mode disrupting mutant PYD constructs (R41A and D48A) were fused with the green fluorescent protein, whereas the WT PYD construct was labeled with a red fluorescent protein and their combinations were coexpressed in HEK293T cells. The experiment had three potential outcomes as illustrated in Figure 6A: in the first case (case I), only the intact surface but not the mutant surface of type I mode deficient PYD would be capable of interacting with the WT PYD filaments. In the absence of alternative interaction modes, competition between the mutant and WT PYDs would occur and therefore inhibition of WT PYD filament formation would be expected. In the second case (case II), we would expect to observe co-localization of type I mode deficient PYD on the WT PYD filaments without any inhibition of the WT PYD filament formation. This scenario could only be possible if type I mode-deficient PYD used alternative interaction modes to bind to the WT PYD filaments. In the last case (case III), type I mode-deficient PYD would not colocalize on the WT PYD filaments, and the WT PYD filament formation would not be affected. In this case, the mutation on PYD might exert its effects on multiple interaction surfaces.

We exploited type I mode-deficient R41A and D48A mutant PYDs to find out whether type I is the only interaction mode for the PYD of ASC. EGFP-labeled R41A and D48A mutant PYDs did not form filaments and displayed a diffused expression pattern throughout the cell when expressed one by one (Figures 5B and 6B). However, when these constructs were cotransfected with the mCherry-labeled WT PYD, the D48A mutant PYD fully colocalized on the WT PYD filaments, suggesting the presence of alternative interaction modes according to case II (Figure 6C; Movie S1D). The R41A PYD only partially colocalized with the WT PYD filaments at spots where the WT PYD filaments were dense. The experimental outcome for the R41A PYD was intermediate between cases II and III, indicating that the effect of R41A mutation is not limited to type I interaction mode surfaces only.

We confirmed the colocalization of the R41A and D48A mutant PYDs on the WT PYD filaments by an in vitro FRET experiment (Figures 6D and 6E). Briefly, the same set of plasmids as in Figure 6C were cotransfected into HEK293T cells and relative efficiency of FRET from the R41A and D48A mutated EGFP-labeled PYDs to the mCherry-labeled WT PYD filaments were measured. Relative FRET efficiency is inversely proportional to the distance between FRET donor (EGFP) and acceptor (mCherry). EGFP-PYD WT and EGFP alone were used as positive and negative controls, respectively. In accordance with the co-localization data, both R41A and D48A mutant PYDs had significantly higher relative FRET efficiencies compared to the negative control, EGFP alone. Relative FRET efficiency of the D48A mutated PYD was also closer to, although slightly lower than the positive control, EGFP-PYD WT. Proper expression of FRET constructs were checked by western blotting (Figure 6F).

The present finding on multiple interaction modes for PYD concurs with the recent cryo-EM structure (Lu et al., 2014). Next, we checked the significance of these two amino acids with respect to the dynamics and interactions of PYD.

Global Hinges Control PYD-PYD Interactions

The global motion of PYD was determined by the GNM. The slow modes of dynamics are implicated as functional (Bahar and
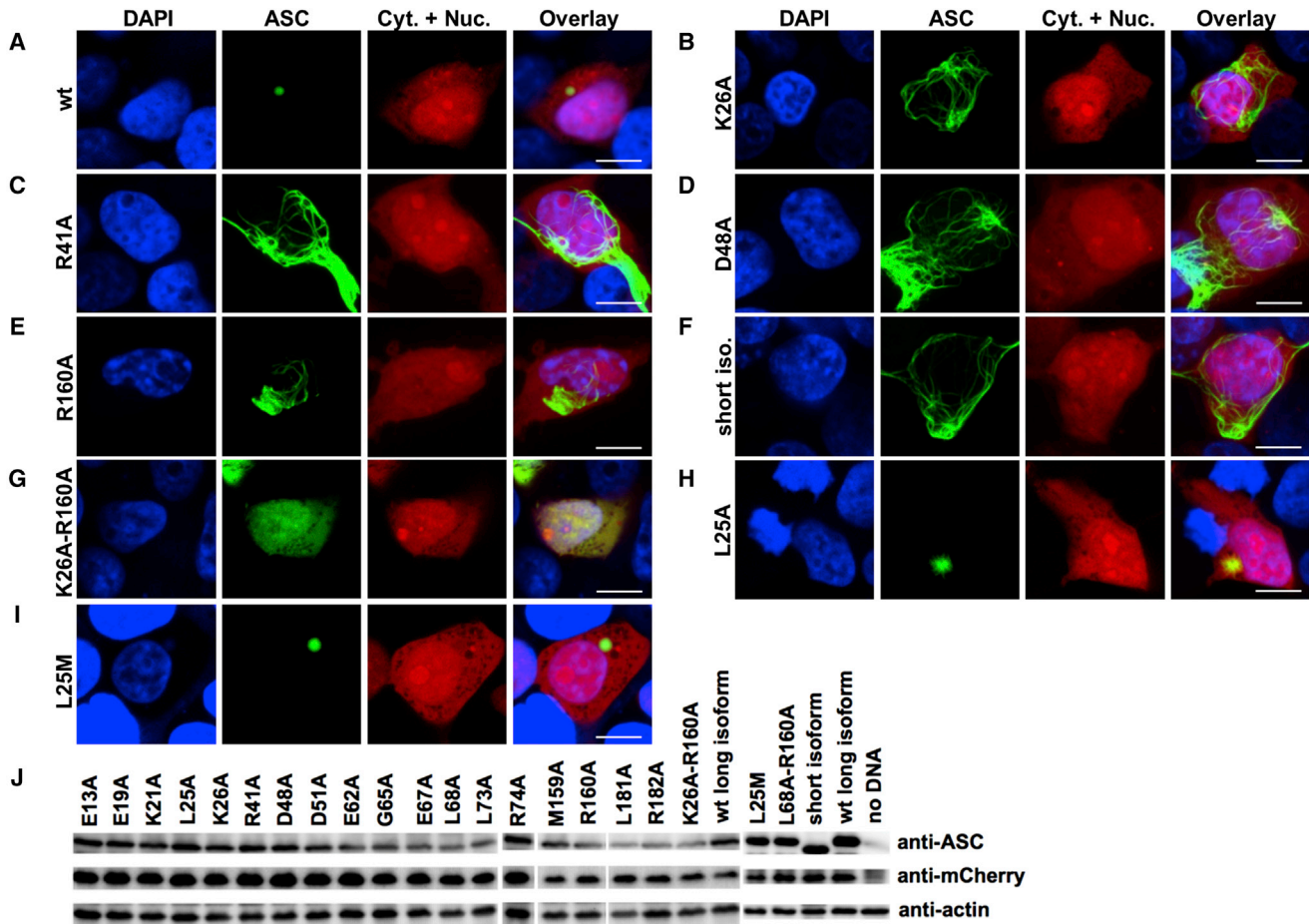
Figure 4. Selected Mutations in ASC PYD and/or CARD Disrupt ASC Speck Formation
EGFP-ASC variant encoding plasmids were transfected into HEK293T cells. Indicated site-directed mutations were created on the long isoform of ASC. Representative confocal micrographs of ASC variants are shown in (A)–(I).
(A) WT long isoform.
(B) K26A.
(C) R41A.
(D) D48A.
(E) R160A.
(F) Short isoform.
(G) K26A-R160A.
(H) L25A.
(I) L25M. Nucleus was stained with DAPI. Whole cells (cytosol + nucleus) were depicted by cotransfection of mCherry encoding plasmid. Scale bar represents 10 μm. Wide-field images of indicated ASC variants are shown in Figure S1D and the complete list of ASC variant phenotypes is given in Table 1.
(J) Western blotting analysis of cells transfected with indicated ASC variants. Anti-mCherry and anti-actin are used as transfection and loading controls, respectively. See also Figure S1.

Rader, 2005). Hinges are mechanistic sites that control the global modes of motion and cooperative fluctuations. The slowest GNM mode divides PYD into two dynamic domains (H1, H4, H5, and H6 [blue] and H2, H3, and the H2 and H3 loop [red]; Figure 3A) by the hinge sites at E13-L20, M47-A49, and S58-Y60. D48 is a hinge amino acid and part of the hinge axis/plane that controls the global motion of PYD and the cooperativity between its dynamic domains. The perturbation introduced with D48A may affect the allosteric interaction of the two surfaces of type I interaction mode; H1 and H4 being at one dynamic domain and the opposite surface H2 and H3 being on the other. On the other hand, R41 is at a hinge site of the second slowest mode

of PYD; the two dynamic domains in this mode (the N-terminal half of H1, the H2 and H3 loop, the C-terminal half of H4, H5, and H6 [blue] and the C-terminal half of H1, H2, H3, and the N-terminal half of H4 [red]; Figure 3B) is defined by the hinge sites at I8-L12, L28-V30, R38-P40, K55-L56, and E62-A66. This may imply that the binding may not be only a local phenomenon here.

Consistent with the effect of single point mutations on the assembly of the ASC speck and PYD filaments (Figures 4 and 5), E13, E19, K21, R41, and D48 are associated with the hinges of the PYD's global motion. This provides a mechanistic perspective for these amino acids and their possible allosteric effects though the global mode perturbation in addition to local effects.
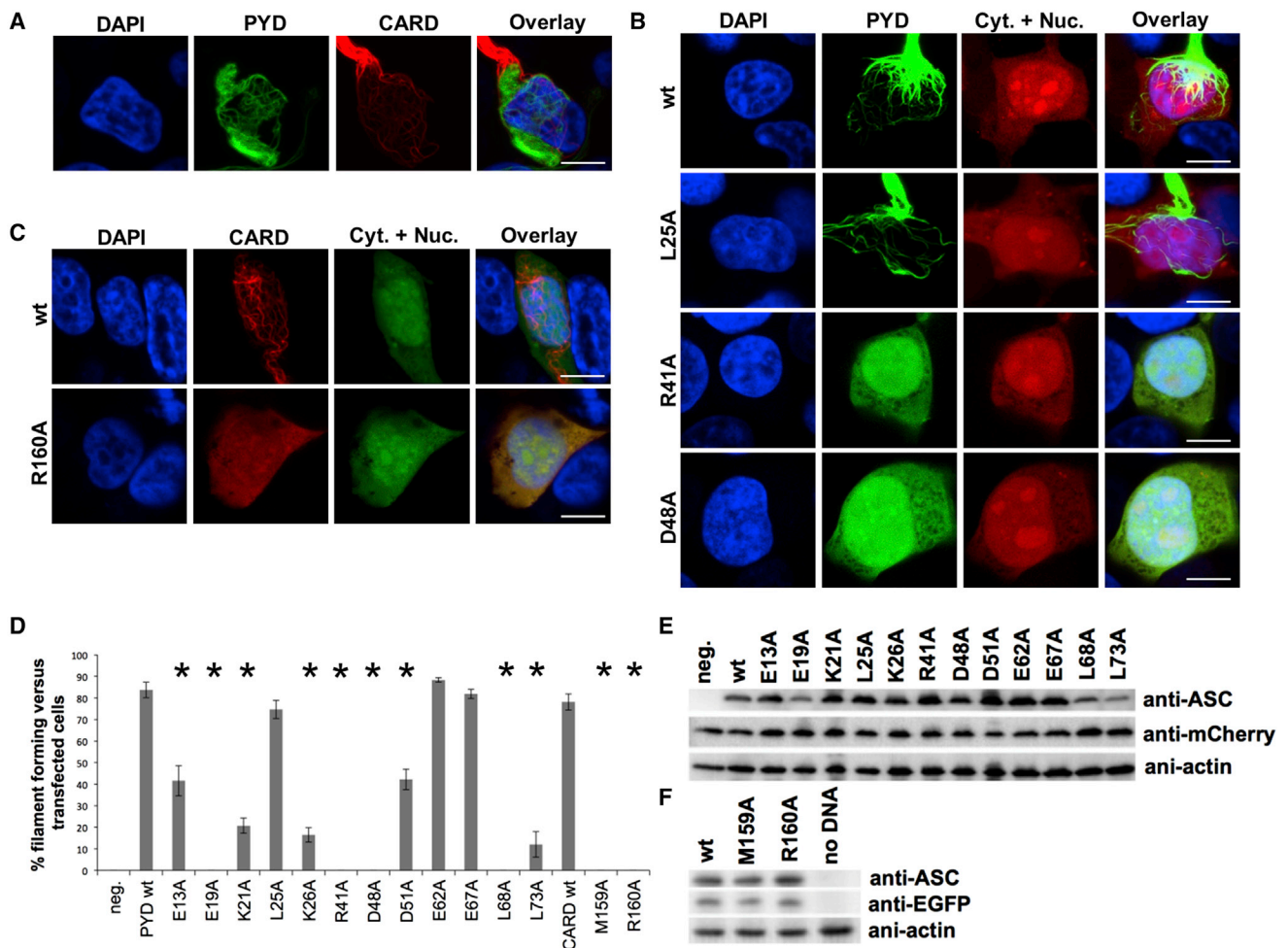
Figure 5. ASC Speck Disrupting Mutations Inhibit the Filament Formation of Individual PYD and CARD

(A) EGFP-PYD and mCherry-CARD constructs were cotransfected into HEK293T cells.

(B–D) An overlapping set of mutations as in Table 1 was created on EGFP-PYD (B) and mCherry-CARD (C) constructs. (B) Representative images of four EGFP-PYD constructs (WT, L25A, R41A, D48A) are shown. (C) Representative images of two mCherry-CARD constructs (WT and R160A) are shown. Nucleus was stained with DAPI. Whole cells (cytosol + nucleus) were depicted by cotransfection of mCherry- and EGFP-encoding plasmids in (B) and (C), respectively. Scale bar represents 10 μm. See also Movie S2. (D) Mutated EGFP-PYD- and mCherry-CARD-encoding plasmids were transfected into HEK293T cells. Ratios of filament forming cells versus transfected cells were calculated (stars: p < 0.001). Three fluorescent wide-field images were analyzed for each construct (>1,000 cells per construct). See also Table S1.

(E and F) Cells in (D) were analyzed by western blotting. Anti-actin: loading control. Anti-mCherry and anti-EGFP are transfection controls in (E) and (F), respectively. neg. (negative control), EGFP alone. The error bars represent one SD.

R41A and D48A Affect the PYD's Dynamics and Cooperativity

Both R41A and D48A led to the type I-deficient mutant PYDs and disrupted the speck formation of the full-length ASC protein. D48 is not directly involved in any type of interaction modes as an interface residue in the new cryo-EM structure (Lu et al., 2014). On the other hand, R41 is a binding site in both type I and type III interaction modes by making two H-bonds with D54 and nonbonded contacts with E13, N14, and T16, respectively. To further understand the interaction modes of PYD, molecular dynamics (MD) simulations of the WT, R41A, and D48A mutant PYDs were also carried out to view the changes in the internal dynamics along the structure of PYD with the mutations. Neither mutation led to significant conformational changes in PYD. The sampled MD conformations remained within 2 Å root-mean-square deviation in both WT and mutant PYDs (Figures S3A–S3C), implying mainly an entropic nature in the observed behavioral changes with the dynamic view presented below.

The residue mobility and flexibility profiles were similar between the WT PYD and both mutant PYD (Figures S3D–S3F, S3J, and S3K). Nevertheless, D48A stabilizes the fluctuations of the loop H4 and H5, which forms one of the surfaces of type II interaction mode (Figures S3G–S3I). This also holds for the flexibility. D48, being a hinge residue, allosterically affects the dynamic space of the loop H4 and H5. On the other hand, the dynamic network—the network of correlated fluctuations—within PYD showed significant differences among WT, R41A, and D48A PYD (Figure 7) and apparently led to different dynamic
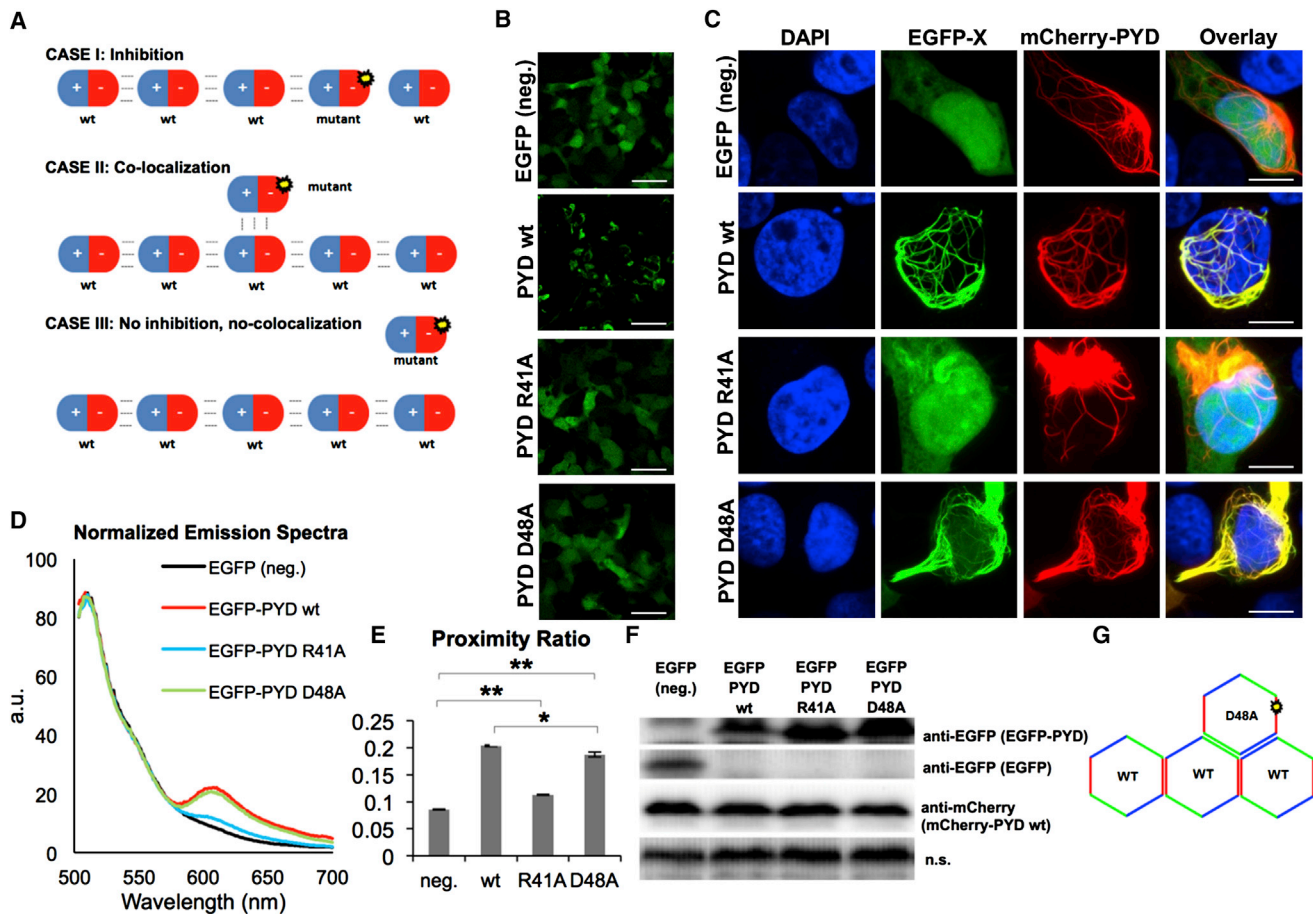
Figure 6. Alternative Interaction Modes of the PYD of ASC

The presence of alternative interaction modes (other than type I) was investigated using type I mode deficient PYD constructs. For this experiment, WT and type I deficient PYDs labeled with different colored fluorescent markers were cotransfected into HEK293T cells.

(A) Potential outcomes of our experimental setup are schematically described. Type I interaction surfaces of PYD are depicted as blue (+) and red (−) in the cartoon model, representing their electrostatic surface potentials. Dashed lines represent interactions between PYDs. Yellow star stands for the mutation on type I mode deficient PYD.

(B) Wide-field images of cells transfected with plasmids encoding EGFP (negative control), EGFP-PYD WT (positive control), EGFP-PYD R41A, and EGFP-PYD D48A. Scale bar represents 50 μm.

(C) mCherry-PYD WT-encoding plasmid was cotransfected with EGFP (negative control), EGFP-PYD WT (positive control), R41A- and D48A-encoding plasmids. DAPI, nucleus. Scale bar represents 10 μm. See also Movies S1A, S1B, S1C, and S1D.

(D) Cells were cotransfected as in (C). The graph shows emission spectra of cell lysates upon excitation at 488 nm (donor excitation maximum), normalized with emission maximum of EGFP. Samples were measured twice and cells were transfected in duplicate.

(E) Relative FRET efficiencies (proximity ratio) of cell lysates in (D). **$p < 0.0013$, *$p < 0.042$.

(F) Western blotting analysis of cell lysates in (E).

(G) Proposed model for colocalization of PYD D48A on PYD WT filaments. Red edges: type I interaction surfaces. Green and blue edges: alternative interaction surfaces. The error bars represent one SD.

fluctuations with respect to the binding interactions. We mainly explore the cooperativity between the surfaces of the interaction modes on separate PYD.

In the WT PYD, there are positively correlated fluctuations between H1 and H2 (particularly between I8, L12, and E13 on H1 and K21-L27 on H2), indicating allosteric communication between the opposite surfaces of type I interaction mode. Both H1 and H2 display weak coupling with H5 (Figures 7A and B), where H5 also slightly correlates with H4. H1 and H4 are at one of the type I interaction mode surfaces and are weakly correlated. Additionally, there is also a coupling between R41

(N terminus of H3) and K55 (H4) of still two opposite surfaces where R41 and D54 forms an interchain H-bond in type I interaction mode during oligomerization (Lu et al., 2014). On the other hand, there is moderate and no visible cooperativity between type II (C terminus of H4 and the loop of H4 and H5 with loop of H5 and H6) and type III (the loop of H1 and H2 and loop of H2 and H3) interaction mode surfaces, respectively (Figures 7C and D).

D48, being a global hinge, was able to lead to a dynamic change in the cooperativity of PYD with the mutation (Figure 3A). The correlations of H1-H2, H1-H4, and H1-H5 disappear with a
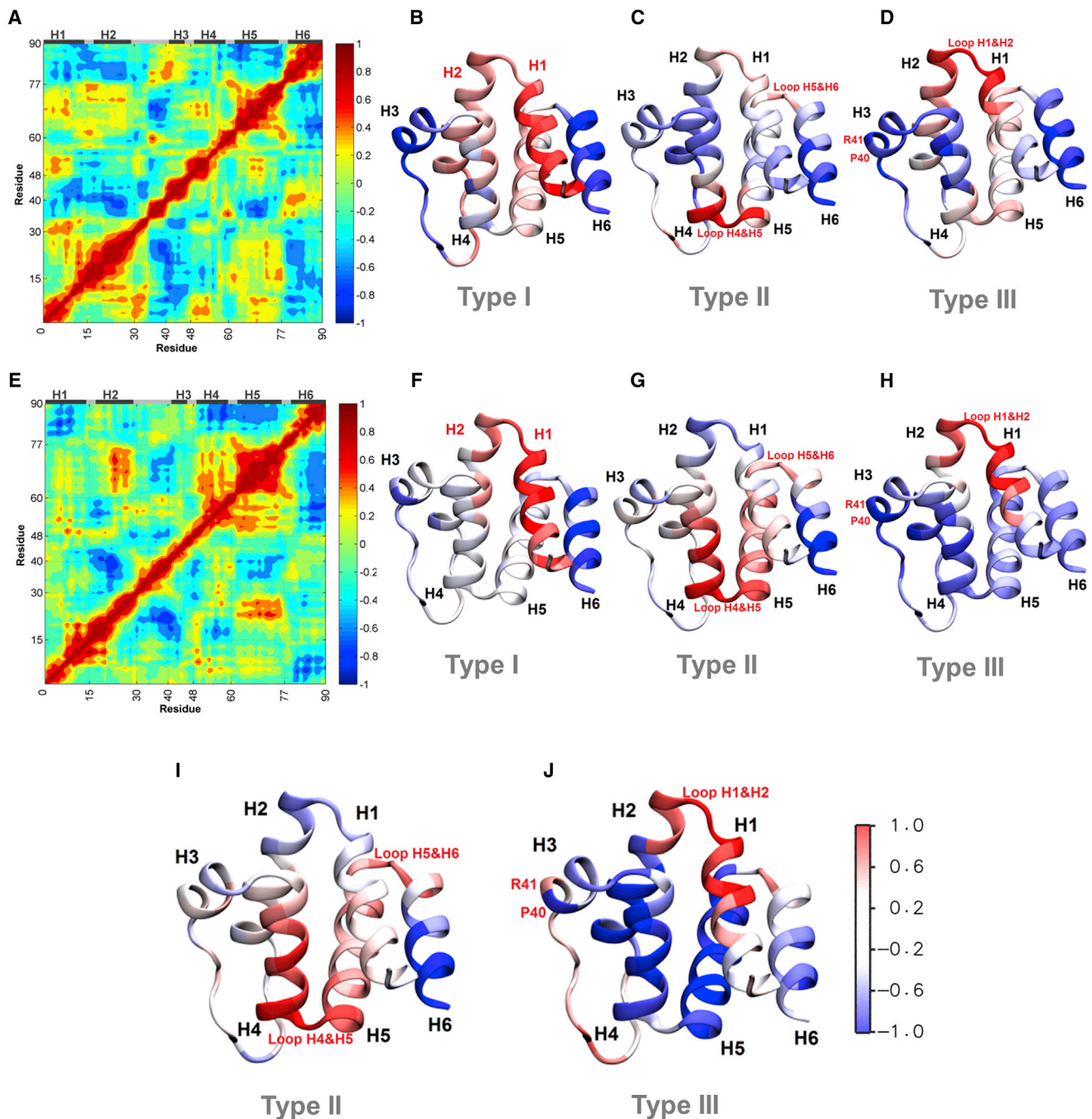
Figure 7. Correlation between Amino Acid Fluctuations of the WT and D48A PYD by MD Simulations

(A–D) The correlation map of the WT PYD (A): the average correlation of one of the surfaces of the type I (I8-E13) (B), type II (V57-F62) (C), and type III (E13-T16) (D) interactions modes with the rest of WT PYD color-coded.

(E–H) The correlation map of the D48A PYD (E): the average correlation of one of the surfaces of the type I (I8-E13) (F), type II (V57-F62) (G), and type III (E13-T16) (H) interactions modes with the rest of the D48A PYD color-coded.

(I and J) The average correlations of the type II (V57-F62) (I) and type III (E13-T16) (J) interaction modes, when the D48A PYD MD simulation runs are clustered based on the correlation strength of the two opposing surfaces of the type II (four runs) and type III (two runs) interaction modes. The residue stretches for each of the interaction mode surfaces were chosen based on the most significant differences between the WT and D48A PYD observed. The results also for R41A are given in the Supplemental Experimental Procedures. See also Figures S3–S5.

decrease in the correlation of R41 and K55. Moreover, the correlation of H2-H5 and H4-H5 significantly increases (Figure 7E). Interestingly, the increased cooperativity of H4-H5 leads to an in-

crease in the correlations between H4/the loop of H4 and H5 and loop of H5 and H6, which describes the type II interaction mode (Figures 7C and 7G). The dynamics of the H4 and H5 loop

(Figures S3G–S3K) should also corroborate this behavior. Furthermore, the analysis of the individual D48A PYD MD simulation runs revealed that there is an adverse behavior between the type II and type III interaction modes. Although the type II interaction mode dominates in the average behavior (Figure 7G), when D48A PYD MD simulation runs are clustered based on the relative strength of the cooperativity of the type II and III interaction mode surfaces, the type II and type III interactions mode is stronger while the type III and type II interaction mode is weaker, respectively, in four and in two of six MD simulation runs (Figures 7I and 7J; Figure S4M). As a result, when the correlation maps are averaged based on the latter groups of MD simulation runs, a stronger type II/type III interaction mode evolves (Figures S4A–S4H). An interesting point to note here is that one of the surfaces of each interaction mode displays a coupling in the WT, which is lost with the D48A PYD.

R41A could affect binding interactions globally as being a hinge residue (second slowest mode) and locally as an interface residue in both type I and type III interaction modes. The dynamic cooperativity of R41A PYD compared to WT PYD displays that the correlation of the type I interaction mode surfaces H1-H2 decreases and H1-H4 disappears, and the correlation of H2-H5 increases (Figure S4I). However, the latter changes are not as significant as observed in the D48A PYD (Figure 7E). With this network of cooperativity, neither of the type II and type III interaction mode surfaces significantly appear (Figures S4K and S4L). R41 is an important conserved position in pyrin PYD (R42). R42W in pyrin PYD is associated with familial Mediterranean fever (Vajjhala et al., 2014).

Taken together, both D48A and R41A affect the dynamic network of the protein, although this does not exclude the expected local perturbations. D48A significantly affects the type I interaction mode and disposes the type II and/or type III interaction modes. Nevertheless, R41A cannot reveal the alternative interaction modes, which may explain the behavioral differences between D48A and R41A in the colocalization experiments (Figure 6C). There appears to be an interplay among different interaction modes revealed by D48A, which may suggest an order in the use of different type of interaction modes during the filament formation. It is interesting to note here that the filament disrupting mutations except D48A that is not an immediate binding residue are hinges at the binding interfaces. The association of hinge dynamics with binding infers allostery and long-range control in the oligomerization.

L25 is an interaction site in the type I interaction mode but L25A does not disrupt the filament formation. It makes nonbonded contacts with L50, T53, and D54 on H4 of the other PYD monomer during oligomerization (Lu et al., 2014). Furthermore, L25 is close to R41 and correlates with I8 (and L12, E13) at the opposite surfaces of type I interaction mode in the WT PYD. R41 and I8 are the hinges of the second slowest mode. The latter correlation disappears in D48A PYD and also weakens in R41A PYD. To this end, the effect of L25A surrounded by charged residues on the PYD's interactions could be a weak direct effect and/or a secondary effect through R41 and I8.

Finally, the projection of the MD-sampled conformations onto the three principal components shows that similar conformers are observed in the WT and mutant PYD, but mutations induce an effect in the dynamic ensemble by changing the populations of the various subspaces, mainly of the first principal motion (Figures S5A–S5C). The distribution of the GNM eigenvalues in the two slowest modes of the MD-sampled conformations was analyzed to further reflect the changes in the dynamics of the WT and mutant PYD (Figure S5D) (Hall et al., 2007). A slight shift is observed to the lower and higher eigenvalues, respectively, with the D48A and R41A PYD compared to the WT structure. Lower eigenvalues means higher cooperativity for D48A. Lower cooperativity of R41A may relate to its potential that may affect all modes of interactions.

DISCUSSION

The discovery of the micrometer-sized perinuclear structure formed by ASC proteins, namely the ASC speck, precedes the finding that the ASC protein acts as an adaptor in various inflammasomes (Latz et al., 2013; Masumoto et al., 1999). Subsequent studies suggested this structure as the activation platform for inflammasome activity (Fernandes-Alnemri et al., 2007). Regardless of its function, the ASC speck shares similarities with aggresomes and aggresome-like structures, and it is thus frequently referred to as an aggregate. It was an open question whether the ASC speck formation is a result of specific interactions by PYD and/or CARD or via nonspecific hydrophobic interactions in the more conventional way that the aggregate formation occurs.

The results of our mutation screen on the full-length ASC show that the first scenario is more likely. We demonstrate that mutations inhibiting the PYD-PYD and CARD-CARD interactions are disrupting the ASC speck as well (Figure 4). Furthermore, the ASC-disrupting mutations are plausible binding amino acids based on the intrinsic dynamics of PYD and CARD and the amino acids that are key in the global dynamics of PYD. If the ASC speck formation was merely a result of aggregation of ASC proteins from their hydrophobic patches, we would expect to observe little or no difference when we mutate amino acids that are considered intrinsically important for the dynamics or specific PYD-PYD and CARD-CARD interactions, which is the opposite of our observation. Innate immune pathways are characteristically fast responding, such as NF-κB activation, to perform their first line of protection (Wang et al., 2002). Formation of the ASC speck via specific PYD and CARD interactions may explain its rapid assembly, which only takes minutes compared to the hours-long aggresome formation process (Cheng et al., 2010).

The ASC Speck Should Be Considered a Polymer or a Scaffold Made of Polymers
Our results are consistent with a previous mutation screen study (Vajjhala et al., 2012) that used coimmunoprecipitation (coIP) and GST pull-down assays. Cumulative results reinforce the idea that the ASC speck formation is based on specific interactions rather than protein aggregation: coIP and GST pull-down assays showed that E13A, K21A, K26A, R41A, D48A, and D51A mutations disrupted specific interactions between PYDs (Table S1). We observed that these mutations on PYD constructs disrupted filament formation and disrupted ASC specks when they were present in full-length ASC constructs. If it were the case that the ASC specks were formed by nonspecific aggregation of

ASC proteins, we would not see any effect of single mutations inhibiting specific interactions of PYD and CARD on the assembly of the ASC speck. We suggest the term polymer or polymer scaffold instead of aggregate for the ASC speck because the term has been coined for PYD filaments recently (Cai et al., 2014; Lu et al., 2014).

It is general assumed that PYD- and CARD-containing proteins interact via homotypic PYD-PYD and CARD-CARD interactions. Separate PYD and CARD were expressed in the same cell and mutually exclusive filament formation was observed (Figure 5A). Nonoverlapping PYD and CARD filaments show the specificity of filament formation. On the other hand, our study is in conflict with a previous study that shows heterophilic interactions between PYD and CARD (Masumoto et al., 2001). A previous mutational screen study on separate PYD using loss-of-filament-formation as an output (Moriya et al., 2005) also presented conflicting results with our study for mutations E13A, L25A, E62A, E67A, and L73A (Table S1). Finally, another recent study focusing on the CARD of ASC identified an overlapping amino acid important for the ASC speck formation, R160 (Proell et al., 2013). However, the shape of the structure upon disruption of the ASC speck was not mentioned as filaments, probably due to low image magnification.

Alternative Modes of PYD-PYD Interaction Facilitate Polymerization

PYD and CARD belong to the death-fold domain superfamily. Another member of this superfamily, death-domain used at least three nonoverlapping interaction modes according to the crystal structures of DISC, MyDDosome, and PIDDosome complexes (Kersse et al., 2011; Lin et al., 2010; Park et al., 2007; Wang et al., 2010). A recent mutagenesis study proposed that the PYD filament formation may be a result of type I interactions (Vajjhala et al., 2012). The simple observation of the PYD and CARD filaments' branching in the cytosol indicates that type I might not be the only interaction mode effective in these domains (Figures 5A–5C and 6C; Movies S1B and S2). This idea was further supported by the colocalization of type I mode-deficient D48A PYD on the WT PYD filaments. We confirmed the degree of colocalization with an in vitro FRET experiment, which showed that the D48A PYDs interacting with the WT PYD filaments have a close relative FRET efficiency compared to the positive control. Interestingly, coIP and GST pull-down experiments showed that the D48A PYD fails to interact with the WT PYD (Vajjhala et al., 2012), indicating that type I interaction is abolished by D48A mutation. Note that coIP and GST pull-down assays evaluate interactions between soluble proteins. However, colocalization and in vitro FRET (using whole cell lysate) experiments take insoluble PYD filaments into account. Cumulative results point out that the mutant PYD (D48A) is not able to interact with the WT PYD monomer but can have an interaction with insoluble WT PYD filaments. This result can be explained by a model in which the binding interface of filaments composes more than two PYDs (Figure 6G). The recent cryo-EM-based structure of PYD filaments also supports the presence of alternative interaction modes of PYD (Lu et al., 2014). Interestingly, R41 was depicted on both type I and type III interaction surfaces in this model. Such a configuration is in good agreement with our experimental results, explaining why R41A PYD (unlike D48A

PYD) was only poorly able to interact with WT PYD filaments (Figures 6C–6E).

It is remarkable that PYD-PYD interaction inhibiting mutations have a gradual effect on filament formation frequency rather than an all-or-none phenotype. We can explain this observation by the increase of threshold concentration required for nucleation of PYD filaments. This theory is consistent with recent studies showing prion-like polymerization of PYD filaments (Cai et al., 2014; Lu et al., 2014). On the other hand, R41A and D48A mutations completely destroy filament formation, indicating these mutants are severely defected in type I interaction mode. Thus, ability of the D48A PYD to interact with the WT PYD filaments can be explained by presence of non-type I interactions in PYD filaments. The cryo-EM structure of PYD filament was published while our manuscript was in preparation, confirming alternative interaction modes on PYD filaments (Lu et al., 2014).

Combined analysis of the GNM and MD simulations described the roles of R41A and D48A in the PYD's dynamics and revealed the allosteric nature of the binding interactions. The two surfaces of the interaction modes indeed show a dynamic coupling on separate PYD. The allosteric dynamics, although favoring type I interaction mode in the WT PYD, supports type II and type III interaction modes in the D48A PYD, which implies an interplay between different types of interaction modes that could be controllable through global dynamics. This might also imply that the type I interaction mode forms the first level compaction of PYD-PYD filament formation and may predispose type II and type III interaction modes for the next level compaction.

Our results prove that specific interactions by PYD and CARD are critical for the ASC speck formation. Furthermore, the flexible linker between the PYD and CARD of ASC is also essential for the globular ASC speck formation. The alternative splice variant of ASC (short isoform) lacks this linker and fails to form the ASC speck but forms filaments instead (Figure 4F). NMR structures of full-length ASC reveal that the linker can acquire a variety of conformations, which might serve the basis of conformational flexibility of ASC to use different interaction modes in the highly compact ASC speck.

The ASC Speck Formation Requires at Least Two Distinct Levels of Compaction

L25A mutant full-length ASC displayed an atypical phenotype, called Medusa's head in this study. It is a perinuclear structure with a size close to the ASC speck but has short filaments radially pointing outward from its core (Figure 4H). Interestingly, the mutation appears to have no effect on the PYD-PYD interactions according to our PYD filament formation assay (Figures 5B and 5D) and coIP/GST pull-down experiments by another group (Vajjhala et al., 2012). It seems that L25A mutated full-length ASC suffers a deficiency in the compaction of the ASC speck. We suggest that L25A and rest of the mutations disrupting the ASC speck (e.g., D48A on PYD and R160A on CARD) interfere with disparate levels of compaction, which supports the idea that the ASC speck is an organized scaffold instead of a nonspecific aggregation of ASC proteins. According to our model, the ASC speck formation is based on at least two levels of compaction: the first level is based on homophilic interactions between the PYD-PYD and CARD-CARD, followed by the second level of compaction, which can be inhibited by L25A mutation. The presence of

alternative interaction modes in PYD (and possibly in CARD as well) might explain how the PYD and CARD filaments organize in the ASC speck at the second level of compaction.

The importance of dynamics in the function has been highlighted with the prediction and explanation of most of the mutations that affect the speck formation by the full-length ASC and the filament formation by separate PYD.

EXPERIMENTAL PROCEDURES

Molecular Cloning

The pEGFP-C3-hASC plasmid, which encodes a fusion protein of EGFP and human ASC (NP_037390.2), was obtained by subcloning the cDNA of ASC from the pcDNA3-hASC into pEGFP-C3 plasmid using HindIII and EcoRI restriction sites. Site-directed mutations were introduced into pEGFP-C3-hASC plasmid using a PCR-based approach. Double mutations carrying EGFP-ASC constructs (K26A-R160A and L68A-R160A) were cloned sequentially, using EGFP-ASC R160A as a template in the mutagenesis procedure. pEGFP-PYD WT and mutant constructs were further subcloned from pEGFP-C3-hASC variants by amplifying PYD (amino acids between 1 and 90) using PCR and cloning between HindIII and EcoRI sites in pEGFP-C3 empty vector (Clontech). Similarly, pmCherry-CARD wt and mutant constructs were subcloned from pEGFP-C3-hASC variants by amplifying CARD (amino acids between 111 and 195) using PCR and cloning between HindIII and EcoRI sites in the in-house produced empty vector pmCherry-C3.1. Short isoform of ASC (NP_660183.1) was cloned using two-step PCR procedure. First, exon 1 and 3 were amplified and purified, followed by fusion of two fragments via overlapping primer ends in the second step PCR. The fragment was cloned into pEGFP-C3 vector between HindIII and EcoRI sites.

FRET Analysis

For fluorescence resonance energy transfer (FRET) analysis, 15×10^6 HEK293T cells were seeded on 150 mm plates and transfected with 12 μg of indicated plasmids via calcium-phosphate method. Cells were scraped and sonicated in PBS containing protease inhibitor cocktail and 2 mM EDTA. Lysates were transferred to quartz cuvettes and analyzed using a spectrofluorometer (Cary Eclipse, Agilent Technologies). Samples were excited at 488 nm (excitation maximum of FRET donor). See the Supplemental Experimental Procedures for relative FRET efficiency calculation.

Imaging

Cells were observed either using an inverted fluorescent microscope (Axio Observer, Zeiss) or confocal microscopy (TCSSP5II, Leica). For confocal microscopy, cells were seeded on sterile glass coverslips in six-well plates before transfection. Cells were fixed in 4% paraformaldehyde solution for 5 min. The nucleus was stained with 5 μg/ml DAPI for 15 min.

Gaussian Network Model

The GNM (Bahar et al., 1998; Haliloglu et al., 1997) is an elastic network model, where each node is an amino acid represented by its alpha carbon atom (Cα). The interactions between Cαs (within a cut-off radius) are described with harmonic springs as edges. High-frequency fluctuating residues as well as hinge residues were determined by the GNM where high-frequency modes (fast modes) refer to localized fluctuations and low-frequency modes (slow modes) represent global functional motions. All the details about the GNM analysis are given in the Supplemental Experimental Procedures.

Molecular Dynamics Simulations and Analysis

MD simulations were performed with NAMD 2.7 (Phillips et al., 2005) with CHARMM27 forcefield (Brooks et al., 1983) at 310 K and 1 atm using a 2-fs time step. Langevin thermostat and barostat (Phillips et al., 2005) were used to enforce constant temperature and pressure. The PYD structure was obtained from the NMR structure of full-length ASC (PDB ID: 2KN6) (de Alba, 2009). Amino acid mutations were carried out with VMD 1.9.1 (Humphrey et al., 1996). Analysis of the MD trajectories was performed by VMD 1.9.1 and the *ptraj* module of AMBER 11 (Case et al., 2010). Backbone rotational/dihedral fluctuations were calculated using the circular statistics toolbox of

MATLAB (Berens, 2009). Principal components and correlations between residue fluctuations were calculated using MATLAB. The details about the simulated systems, the MD simulations performed, and the analysis are given in the Supplemental Experimental Procedures.

SUPPLEMENTAL INFORMATION

Supplemental Information includes Supplemental Experimental Procedures, five figures, two tables, and two movies and can be found with this article online at http://dx.doi.org/10.1016/j.str.2014.09.011.

AUTHOR CONTRIBUTIONS

T.H and N.O. planned and supervised the project. A.C.S designed and performed mutagenesis, imaging, FRET and western blot experiments. F.S. performed GNM calculations, MD simulations, and analysis. A.C.S., F.S., N.O., and T.H wrote the manuscript.

REFERENCES

Bahar, I., and Rader, A.J. (2005). Coarse-grained normal mode analysis in structural biology. Curr. Opin. Struct. Biol. *15*, 586–592.

Bahar, I., Atilgan, A.R., Demirel, M.C., and Erman, B. (1998). Vibrational dynamics of folded proteins: significance of slow and fast motions in relation to function and stability. Phys. Rev. Lett. *80*, 2733.

Balci-Peynircioglu, B., Waite, A.L., Schaner, P., Taskiran, Z.E., Richards, N., Orhan, D., Gucer, S., Ozen, S., Gumucio, D., and Yilmaz, E. (2008). Expression of ASC in renal tissues of familial mediterranean fever patients with amyloidosis: postulating a role for ASC in AA type amyloid deposition. Exp. Biol. Med. (Maywood) *233*, 1324–1333.

Berens, P. (2009). CircStat: a MATLAB toolbox for circular statistics. J. Stat. Softw. *31*, 1–21.

Brooks, B.R., Bruccoleri, R.E., Olafson, B.D., States, D.J., Swaminathan, S., and Karplus, M. (1983). CHARMM: A program for macromolecular energy, minimization, and dynamics calculations. J. Comput. Chem. *4*, 187–217.

Broz, P., Newton, K., Lamkanfi, M., Mariathasan, S., Dixit, V.M., and Monack, D.M. (2010a). Redundant roles for inflammasome receptors NLRP3 and NLRC4 in host defense against Salmonella. J. Exp. Med. *207*, 1745–1755.

Broz, P., von Moltke, J., Jones, J.W., Vance, R.E., and Monack, D.M. (2010b). Differential requirement for Caspase-1 autoproteolysis in pathogen-induced cell death and cytokine processing. Cell Host Microbe *8*, 471–483.

Cai, X., Chen, J., Xu, H., Liu, S., Jiang, Q.X., Halfmann, R., and Chen, Z.J. (2014). Prion-like polymerization underlies signal transduction in antiviral immune defense and inflammasome activation. Cell *156*, 1207–1222.

Case, D.A., Darden, T.A., Cheatham Iii, T., Simmerling, C.L., Wang, J., Duke, R.E., Luo, R., Walker, R.C., Zhang, W., and Merz, K.M. (2010). AMBER 11, *142*. (San Francisco: University of California).

Cheng, J., Waite, A.L., Tkaczyk, E.R., Ke, K., Richards, N., Hunt, A.J., and Gumucio, D.L. (2010). Kinetic properties of ASC protein aggregation in epithelial cells. J. Cell. Physiol. *222*, 738–747.

de Alba, E. (2009). Structure and interdomain dynamics of apoptosis-associated speck-like protein containing a CARD (ASC). J. Biol. Chem. *284*, 32932–32941.

Ertekin, A., Nussinov, R., and Haliloglu, T. (2006). Association of putative concave protein-binding sites with the fluctuation behavior of residues. Protein Sci. *15*, 2265–2277.

Fernandes-Alnemri, T., Wu, J., Yu, J.W., Datta, P., Miller, B., Jankowski, W., Rosenberg, S., Zhang, J., and Alnemri, E.S. (2007). The pyroptosome: a supramolecular assembly of ASC dimers mediating inflammatory cell death via caspase-1 activation. Cell Death Differ. *14*, 1590–1604.

Gross, O., Thomas, C.J., Guarda, G., and Tschopp, J. (2011). The inflammasome: an integrated view. Immunol. Rev. *243*, 136–151.

Haliloglu, T., and Erman, B. (2009). Analysis of correlations between energy and residue fluctuations in native proteins and determination of specific sites for binding. Phys. Rev. Lett. *102*, 088103.

Haliloglu, T., Bahar, I., and Erman, B. (1997). Gaussian dynamics of folded proteins. Phys. Rev. Lett. *79*, 3090.

Haliloglu, T., Seyrek, E., and Erman, B. (2008). Prediction of binding sites in receptor-ligand complexes with the Gaussian Network Model. Phys. Rev. Lett. *100*, 228102–228102.

Hall, B.A., Kaye, S.L., Pang, A., Perera, R., and Biggin, P.C. (2007). Characterization of protein conformational states by normal-mode frequencies. J. Am. Chem. Soc. *129*, 11394–11401.

Hornung, V., and Latz, E. (2010). Critical functions of priming and lysosomal damage for NLRP3 activation. Eur. J. Immunol. *40*, 620–623.

Humphrey, W., Dalke, A., and Schulten, K. (1996). VMD: visual molecular dynamics. J. Mol. Graph. *14*, 33–38, 27–28.

Johnston, J.A., Ward, C.L., and Kopito, R.R. (1998). Aggresomes: a cellular response to misfolded proteins. J. Cell Biol. *143*, 1883–1898.

Jones, J.W., Kayagaki, N., Broz, P., Henry, T., Newton, K., O'Rourke, K., Chan, S., Dong, J., Qu, Y., Roose-Girma, M., et al. (2010). Absent in melanoma 2 is required for innate immune recognition of Francisella tularensis. Proc. Natl. Acad. Sci. USA *107*, 9771–9776.

Kersse, K., Verspurten, J., Vanden Berghe, T., and Vandenabeele, P. (2011). The death-fold superfamily of homotypic interaction motifs. Trends Biochem. Sci. *36*, 541–552.

Landau, M., Mayrose, I., Rosenberg, Y., Glaser, F., Martz, E., Pupko, T., and Ben-Tal, N. (2005). ConSurf 2005: the projection of evolutionary conservation scores of residues on protein structures. Nucleic Acids Res. *33*, W299–W302.

Latz, E., Xiao, T.S., and Stutz, A. (2013). Activation and regulation of the inflammasomes. Nat. Rev. Immunol. *13*, 397–411.

Leemans, J.C., Cassel, S.L., and Sutterwala, F.S. (2011). Sensing damage by the NLRP3 inflammasome. Immunol. Rev. *243*, 152–162.

Liepinsh, E., Barbals, R., Dahl, E., Sharipo, A., Staub, E., and Otting, G. (2003). The death-domain fold of the ASC PYRIN domain, presenting a basis for PYRIN/PYRIN recognition. J. Mol. Biol. *332*, 1155–1163.

Lin, S.C., Lo, Y.C., and Wu, H. (2010). Helical assembly in the MyD88-IRAK4-IRAK2 complex in TLR/IL-1R signalling. Nature *465*, 885–890.

Lu, A., Magupalli, V.G., Ruan, J., Yin, Q., Atianand, M.K., Vos, M.R., Schröder, G.F., Fitzgerald, K.A., Wu, H., and Egelman, E.H. (2014). Unified polymerization mechanism for the assembly of ASC-dependent inflammasomes. Cell *156*, 1193–1206.

Luque, I., and Freire, E. (2000). Structural stability of binding sites: consequences for binding affinity and allosteric effects. Proteins (*Suppl 4*), 63–71.

Masumoto, J., Taniguchi, S., Ayukawa, K., Sarvotham, H., Kishino, T., Niikawa, N., Hidaka, E., Katsuyama, T., Higuchi, T., and Sagara, J. (1999). ASC, a novel 22-kDa protein, aggregates during apoptosis of human promyelocytic leukemia HL-60 cells. J. Biol. Chem. *274*, 33835–33838.

Masumoto, J., Taniguchi, S., and Sagara, J. (2001). Pyrin N-terminal homology domain- and caspase recruitment domain-dependent oligomerization of ASC. Biochem. Biophys. Res. Commun. *280*, 652–655.

Matsushita, K., Takeoka, M., Sagara, J., Itano, N., Kurose, Y., Nakamura, A., and Taniguchi, S. (2009). A splice variant of ASC regulates IL-1beta release and aggregates differently from intact ASC. Mediators Inflamm. *2009*, 287387.

Miao, E.A., Rajan, J.V., and Aderem, A. (2011). Caspase-1-induced pyroptotic cell death. Immunol. Rev. *243*, 206–214.

Moriya, M., Taniguchi, S., Wu, P., Liepinsh, E., Otting, G., and Sagara, J. (2005). Role of charged and hydrophobic residues in the oligomerization of the PYRIN domain of ASC. Biochemistry *44*, 575–583.

Muñoz-Planillo, R., Kuffa, P., Martínez-Colón, G., Smith, B.L., Rajendiran, T.M., and Núñez, G. (2013). K⁺ efflux is the common trigger of NLRP3 inflammasome activation by bacterial toxins and particulate matter. Immunity *38*, 1142–1153.

Natarajan, A., Ghose, R., and Hill, J.M. (2006). Structure and dynamics of ASC2, a pyrin domain-only protein that regulates inflammatory signaling. J. Biol. Chem. *281*, 31863–31875.

Ozbek, P., Soner, S., Erman, B., and Haliloglu, T. (2010). DNABINDPROT: fluctuation-based predictor of DNA-binding residues within a network of interacting residues. Nucleic Acids Res. *38*, W417–W423.

Ozbek, P., Soner, S., and Haliloglu, T. (2013). Hot spots in a network of functional sites. PLoS ONE *8*, e74320.

Park, H.H., Logette, E., Raunser, S., Cuenin, S., Walz, T., Tschopp, J., and Wu, H. (2007). Death domain assembly mechanism revealed by crystal structure of the oligomeric PIDDosome core complex. Cell *128*, 533–546.

Phillips, J.C., Braun, R., Wang, W., Gumbart, J., Tajkhorshid, E., Villa, E., Chipot, C., Skeel, R.D., Kalé, L., and Schulten, K. (2005). Scalable molecular dynamics with NAMD. J. Comput. Chem. *26*, 1781–1802.

Proell, M., Gerlic, M., Mace, P.D., Reed, J.C., and Riedl, S.J. (2013). The CARD plays a critical role in ASC foci formation and inflammasome signalling. Biochem. J. *449*, 613–621.

Qin, H., Srinivasula, S.M., Wu, G., Fernandes-Alnemri, T., Alnemri, E.S., and Shi, Y. (1999). Structural basis of procaspase-9 recruitment by the apoptotic protease-activating factor 1. Nature *399*, 549–557.

Richards, N., Schaner, P., Diaz, A., Stuckey, J., Shelden, E., Wadhwa, A., and Gumucio, D.L. (2001). Interaction between pyrin and the apoptotic speck protein (ASC) modulates ASC-induced apoptosis. J. Biol. Chem. *276*, 39320–39329.

Schroder, K., and Tschopp, J. (2010). The inflammasomes. Cell *140*, 821–832.

Shi, C.S., Shenderov, K., Huang, N.N., Kabat, J., Abu-Asab, M., Fitzgerald, K.A., Sher, A., and Kehrl, J.H. (2012). Activation of autophagy by inflammatory signals limits IL-1β production by targeting ubiquitinated inflammasomes for destruction. Nat. Immunol. *13*, 255–263.

Srimathi, T., Robbins, S.L., Dubas, R.L., Chang, H., Cheng, H., Roder, H., and Park, Y.C. (2008). Mapping of POP1-binding site on pyrin domain of ASC. J. Biol. Chem. *283*, 15390–15398.

Swapna, L.S., Bhaskara, R.M., Sharma, J., and Srinivasan, N. (2012). Roles of residues in the interface of transient protein-protein complexes before complexation. Sci Rep *2*.

Vajjhala, P.R., Mirams, R.E., and Hill, J.M. (2012). Multiple binding sites on the pyrin domain of ASC protein allow self-association and interaction with NLRP3 protein. J. Biol. Chem. *287*, 41732–41743.

Vajjhala, P.R., Kaiser, S., Smith, S.J., Ong, Q.R., Soh, S.L., Stacey, K.J., and Hill, J.M. (2014). Identification of Multifaceted Binding Modes for Pyrin and ASC Pyrin Domains Gives Insights into Pyrin Inflammasome Assembly. J Biol Chem, jbc. M114. 553305.

Wang, T., Zhang, X., and Li, J.J. (2002). The role of NF-kappaB in the regulation of cell stress responses. Int. Immunopharmacol. *2*, 1509–1520.

Wang, L., Yang, J.K., Kabaleeswaran, V., Rice, A.J., Cruz, A.C., Park, A.Y., Yin, Q., Damko, E., Jang, S.B., Raunser, S., et al. (2010). The Fas-FADD death domain complex structure reveals the basis of DISC assembly and disease mutations. Nat. Struct. Mol. Biol. *17*, 1324–1329.

Zhou, R., Yazdi, A.S., Menu, P., and Tschopp, J. (2011). A role for mitochondria in NLRP3 inflammasome activation. Nature *469*, 221–225.